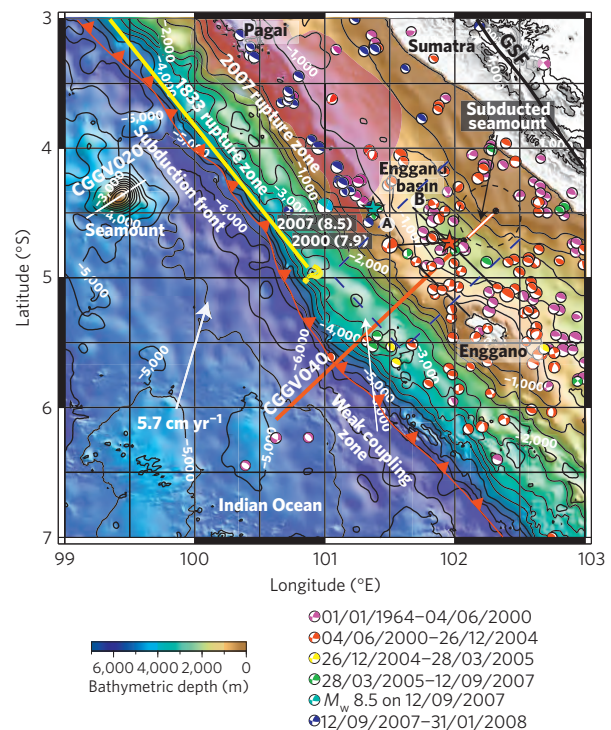


# Aseismic zone and earthquake segmentation associated with a deep subducted seamount in Sumatra

Satish C. Singh<sup>1\*</sup>, Nugroho Hananto<sup>1</sup>, Maruf Mukti<sup>1</sup>, David P. Robinson<sup>2</sup>, Shamita Das<sup>2</sup>, Ajay Chauhan<sup>1</sup>, Helene Carton<sup>3</sup>, Bruno Gratacos<sup>4</sup>, Stephan Midnet<sup>4</sup>, Yusuf Djajadihardja<sup>5</sup> and Heri Harjono<sup>6</sup>

The subduction of large topographic features such as seamounts has been linked to plate locking<sup>1-7</sup>, earthquake generation<sup>8</sup> and segmentation<sup>6</sup>, as well as crustal erosion<sup>9-11</sup> at subduction zones. However, the role of subducted features in the generation of megathrust earthquakes has been difficult to discern because traditional imaging techniques are limited to the upper 12 km of the Earth's crust<sup>12</sup>, whereas these ruptures initiate at depths of 20-40 km (ref. 13). Here we use a deeply penetrating imaging technique with a low-energy source to identify a seamount 3-4 km high and 40 km wide that has been subducted to a depth of 30-40 km below the Sumatra forearc mantle. We find that the seamount has remained intact despite more than 160 km of subduction, and that there is no seismic activity either above or below the seamount. We therefore conclude that the coupling between the seamount and overriding plate is weak and aseismic<sup>14</sup>. We suggest that the subduction of a topographic feature such as a seamount could lead to the segmentation of the subduction zone, which could in turn reduce the maximum size of megathrust earthquakes in these localities.

Our study area lies between the 2007  $M_w = 8.4$  earthquake epicentre<sup>15</sup> and Enggano Island (Fig. 1). Here, the Indo-Australian plate subducts obliquely beneath the Sunda Plate at a convergence rate of  $\sim 57 \text{ mm yr}^{-1}$ , leading to slip partitioning between pure thrust motion orthogonal to the subduction system along the megathrust and strike-slip motion parallel to the subduction system along the Great Sumatra fault on land<sup>16</sup>. The Sumatra subduction zone has been the site of several great earthquakes since December 2004, after more than a century of quiescence for such great earthquakes. However, the area near Enggano Island has been identified as a gap for earthquakes greater than magnitude 8 (ref. 14). GPS studies<sup>14,17</sup> indicate that this could be caused by the presence of a weakly coupled zone that does not have the potential for great earthquakes<sup>16</sup>. The 2007 earthquake initiated at the northwestern extremity of this gap and propagated uni-directionally northward (Fig. 1). The southern limit of the 1833  $M_w \sim 9$  earthquake also lies northwest of the gap<sup>14,17</sup>, coinciding with the lowest bathymetry along the forearc high connecting the Mentawai Islands (Supplementary Fig. S1). Taken together, these observations suggest that this gap plays an important role in the earthquake segmentation process. We acquired a  $\sim 260 \text{ km}$  long deep seismic reflection profile



**Figure 1 | Study area and Sumatra aseismic gap.** Red line: CGGV040 seismic profile. White line bounded by black dots: the positions of the seamount along seismic profile (Fig. 2). The 2007 earthquake rupture zone is in maroon and the blue star its epicentre<sup>15</sup>. The centroid-moment tensor solutions from 1976 to 2008 are plotted at their relocated positions (Supplementary Fig. S3). White line: position of seismic profile CGGV020 shown in Supplementary Fig. S3. The black dashed circle: zone without earthquakes > magnitude 5. Yellow line: 1833 earthquake rupture zone<sup>14</sup>. Blue dashed line: weakly coupled zone<sup>14</sup>. GSF: Great Sumatra Fault. Black lines (A and B) indicate the location of bathymetric profiles shown in Fig. 3.

in this region, traversing the subduction zone orthogonally, and crossing the deformation front in the Indian Ocean, the accretionary wedge, the forearc high, and the forearc basin (Fig. 1).

<sup>1</sup>Laboratoire de Géosciences Marines, Institut de Physique du Globe de Paris, Sorbonne Paris Cité, Paris 75236, France, <sup>2</sup>Department of Earth Sciences, University of Oxford, South Parks Road, Oxford, OX1 3AN, UK, <sup>3</sup>Lamont Doherty Earth Observatory, Columbia University, Palisades, New York 10964-8000, USA, <sup>4</sup>CGGVeritas, Massy 91341, France, <sup>5</sup>Agency for the Assessment and Application of Technology (BPPT), Jl. MH. Thamrin 8, Jakarta 10340, Indonesia, <sup>6</sup>Indonesian Institute of Sciences (LIPI), Jl. Jend. Gatot Subroto 10, Jakarta 12710, Indonesia. \*e-mail: singh@ippg.fr.

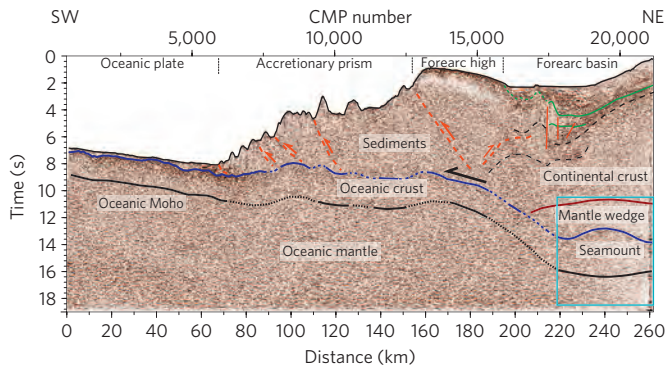


**Figure 2 | Seismic Profile CGGV040.** Interpreted seismic image as a function of two-way travel time. Vertical to horizontal scale is 1:8 on the seafloor. The top of the oceanic crust is marked in blue, oceanic Moho in black, continental Moho in brown, and faults in red. The blue rectangle indicates the part of the data shown in expanded view in Fig. 3. The seamount is identified as a dome-shaped feature between CMP18500 and 21200. The non-interpreted image is shown in Supplementary Fig. S2.

Details of the seismic data acquisition and processing are discussed in the Methods section. The interpreted seismic image as a function of two-way travel time (TWTT) is shown in Fig. 2 and the non-interpreted seismic image in Supplementary Fig. S2. On the oceanic plate, a veneer of thin sediments (200 ms) is present, which gradually thickens to 800 ms at the subduction front. The first 25 km of the frontal part of the accretionary prism consists of folded and faulted accreted sediments sloping gently seaward. The top of the oceanic crust is imaged all along the profile and the oceanic Moho is imaged along a significant part of the profile. The Moho lies about 2 s below the top of the oceanic crust, indicating the crust is about 6 km thick, assuming an average P-wave velocity of  $6 \text{ km s}^{-1}$ , which is consistent with the thickness observed further south<sup>18</sup>.

In the accretionary prism, the sediment thickness increases from 2 s (2 km) near the front to 8 s (12–15 km) beneath the forearc high. There are several landward dipping thrusts between the subduction front and the forearc high, possibly owing to stacking of thrusts landwards. On the northeastern side of the forearc high, there are deep-penetrating, seaward-dipping backthrusts (or backstop) in the forearc basin, which seem to reach the seafloor and form push-up ridges with flower structures, as observed further north<sup>19,20</sup>. A sub-horizontal reflector is imaged at  $\sim 10$  s TWTT (22 km) and is likely to correspond to the continental Moho. Based on several refraction profiles, it is now well accepted that the crust beneath the forearc in Sumatra is thin<sup>18–23</sup>, consistent with our observations. A dome-shaped reflector is imaged at 13–14 s, which seems to be connected with the top of the oceanic crust further SW. The height of this dome is  $\sim 1.1$  s and its width is at least 40 km (Figs 2 and 3). There is a second sub-horizontal reflector at 16 s, which might be the oceanic Moho. If we assume a mantle wedge velocity of  $8 \text{ km s}^{-1}$ , the height of the dome would be 4 km, and the crustal thickness would be 9 km.

This dome-shaped feature could be owing to the presence of a deep subducted seamount or a break-in-slope produced by a thrust fault cutting through the oceanic crust. However, the flat Moho and thick crust beneath the dome suggest that it is owing to a deep subducted seamount (Fig. 3a). A 4-km high and 50-km wide seamount is present on the oceanic plate SW of South Pagai Island, 65 km from the subduction front, indicating that seamounts of such size are present on the subducting oceanic plate (Fig. 1 and Supplementary Fig. S3). The  $\sim 9$  km crustal thickness is similar to the crustal thickness of the seamount observed on the oceanic plate (Supplementary Fig. S3). Although part of the seamount might have been sheared off, a significant part of it has subducted down to 30–40 km depth beneath the forearc mantle.

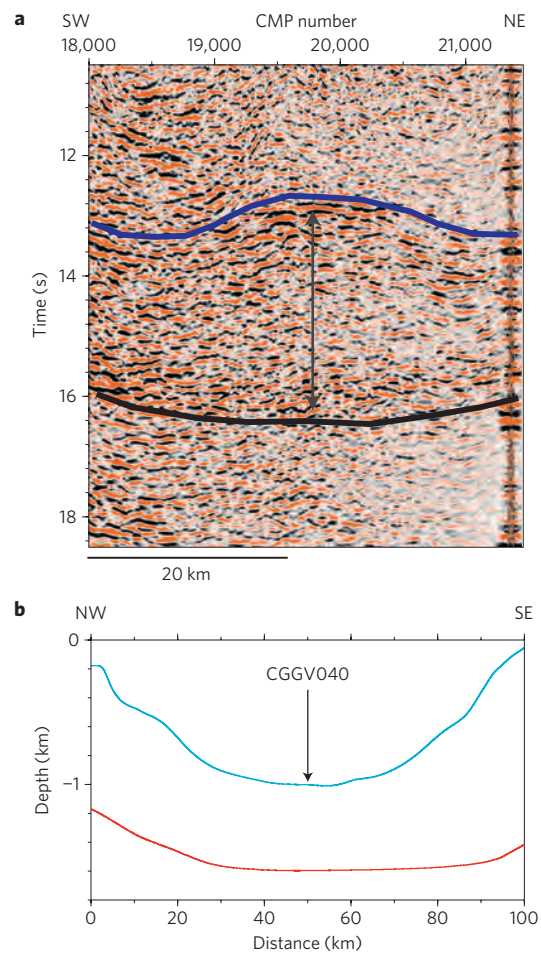


**Figure 3 | Seamount Image and bathymetry profile.** **a**, Expanded view of the subducted seamount imaged on profile CGGV040, shown in Fig. 2. Blue line indicates the top of the seamount. Black line indicates the oceanic Moho. Vertical to horizontal scale is 1:8 on the seafloor. **b**, Seafloor depth along the forearc high (blue) and forearc basin (red) along the profiles marked by A and B shown in Fig. 1. It clearly shows that the deepest point lies along profile CGGV040 along the passage of the seamount.

A complex earthquake of  $M_w = 7.9$ , consisting of strike-slip and thrust sub-events, occurred in 2000 in the downgoing plate<sup>8</sup>, at the southeastern end of the rupture area of the great ( $M > 8.8$ ) 1833 and 2007 earthquakes (Fig. 1). The epicentre of this earthquake lies on our profile in the forearc basin, northeast of Enggano Island (Fig. 1 and Supplementary Fig. S4). Earthquakes before this one were mainly of thrust type. We have relocated all the earthquakes from January 1964 to January 2008 (see Methods section). The seismicity mainly lies beneath the forearc basin, suggesting the deep segment of the subducting plate is active. The 2000 earthquake is in a region showing high seismic activity over the past few decades, although the magnitudes of these earthquakes are small (Supplementary Fig. S4). Its rupture zone is outside and seaward of the seamount. Several aftershocks of the 2000 earthquake are of strike-slip type, but there are also many with thrust mechanisms. It is interesting to note that there is a gap in seismicity both above and below the observed seamount. The gap below the seamount can also be seen in very accurately located earthquakes in this region between 50 and 100 km depths<sup>24</sup>. This is a true gap, as there are earthquakes on either side of the gap at these depths. The diameter of this gap is  $\sim 50$  km, suggesting it is collocated with this seamount.

The bathymetry parallel to the subduction front beneath the forearc high forms an arc of diameter  $\sim 50$  km, with its deepest

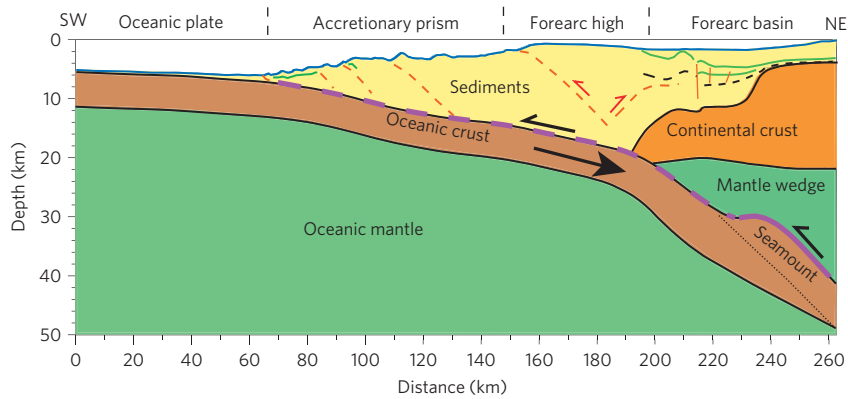


**Figure 4 | Subducted seamount.** Schematic diagram of the subducted seamount, based on the depth-converted image (shown in Supplementary Figs S5 and S6), using a combination of velocity obtained using refraction studies<sup>22</sup> and migration velocity analysis. The solid purple line indicates the pure slip zone above the seamount whereas the purple dashed line indicates the weakly coupled zone. The black dotted line indicates the possible position of the plate interface away from the seamount obtained using hypocenter plots shown in Supplementary Fig. S5.

point along the profile (Fig. 3b). Similarly, the forearc basin is deepest just southwest of the observed seamount and is a saucer-shaped feature, with a length of about 60 km. Although localized bathymetric depressions (furrows) after the passing of seamounts have been observed along the Middle American trench<sup>9,11</sup>, as well as in laboratory experiments on subduction<sup>25</sup>, large-scale symmetric bathymetric depressions after the passing of a large seamount are a new observation. We suggest that these two bathymetric depressions are associated with the basal erosion caused by the passage of the seamount beneath the forearc high and basin, with consequent subsidence of the overriding crust. Subsidence of 700 m in the forearc high would require 1–2 km of upper plate erosion if the subsidence was mainly owing to basal erosion<sup>11,26</sup>. Basal erosion of the mantle wedge and the subsequent subsidence might also explain the complex faulting and deformation of the sediments observed at the up-dip limit of the seamount, which have been interpreted to be owing to backthrusting<sup>19,20</sup> or strike-slip faulting<sup>27</sup>.

The bathymetry low could also be owing to a tear in the downgoing plate along north–south trending fracture zones. A NS fracture zone would produce a triangle-shaped bathymetric anomaly in the upper plate. However, the two bathymetric low anomalies we observe are both orthogonal to the subduction front and symmetric, which could only be produced by a subducting seamount (Fig. 3).

The seamount is located 150–190 km from the subduction front. If we take  $47 \text{ mm yr}^{-1}$  as the subduction rate in the direction orthogonal to the trench<sup>14</sup>, then the seamount would have been at the subduction front around  $\sim 4$  Myr ago. The age of volcanism on the oceanic plate is not well known, but the age of the lithosphere is about 68 Myr (ref. 28), and hence it should be cold. Our study shows that the current position of the seamount is at 30–40 km depth, at the lower limit of the seismogenic zone below the mantle wedge. Furthermore, most of the thrust events outside the seismic gap between 30 and 50 km depth are aligned along the steeply dipping part of the oceanic plate interface between 18 and 30 km depth, suggesting that earthquakes outside the seamount area occur at the top of the plate interface (Supplementary Figs S5 and S6). Steeper dips ( $20^\circ$ – $30^\circ$ ) of the focal mechanisms of these earthquakes give further support to this observation (Supplementary Fig. S5).

Several authors have postulated that observations of patterns of seismicity or earthquake slip distribution indicate that subducted bathymetric highs can act as either locally strong or weak areas of plate interface coupling at subduction zones. Subducted seamounts can act as asperities (an asperity is defined as a protrusion on a surface) to locally increase the coupling at the plate interface by increasing the normal stress across it<sup>1,2</sup>. On the other hand, the entrainment of fluid-rich sediments at the subduction interface

and damage to the overriding plate may reduce the interface coupling<sup>6,11</sup>. Both can lead to the absence of seismicity associated with the seamount. The largest earthquakes on the Costa Rica subduction zone are coincident with subducted seamounts<sup>4</sup>, suggestive of locally increased coupling. Conversely, geodetic and paleogeodetic measurements in the Sumatra region have suggested that the segmentation observed in the megathrust earthquakes is owing to weakly coupled regions that are collocated with topographic features on the subducting seafloor<sup>14</sup>.

It is impossible to know how large the seamount was before subduction, but it is clear that a significant portion of the seamount has survived intact after more than 160 km of subduction. If the coupling between the seamount and overriding plate has been weak throughout its subduction history then this would increase the likelihood of the seamount persisting to depth. Excessive fluid released from thick seamount and fluid-rich sediments above would serpentinize the forearc mantle, leading to pure sliding of the seamount without any seismicity above it. The passage of the subducting seamount and associated basal erosion could produce a tunnel of damaged material at the base of the upper plate, potentially allowing increased fluid migration and leading to weak coupling in the wake of the seamount. The presence of small thrust earthquakes up-dip suggests that this zone is not purely aseismic, and may explain the discrepancy between different coupling models<sup>14,17</sup>. Thus, a passage of a seamount could produce segmentation along the subduction zone, and possibly reduce the maximum size of earthquakes.

The Investigator Ridge, which is the largest topographic feature entering the Sumatra subduction zone, seems to have led to a zone of weak coupling<sup>14</sup> and introduced a complex low bathymetry expression in the accretionary prism; it lies at the southern boundary of the 2005 great Nias earthquake. Our results suggest that, in the absence of any direct deep seismic images of subducted seamounts and geodetic data, seismic gaps in the forearc and bathymetric anomalies could be used to identify possible passages of subducted bathymetric features, and hence to define along-strike segmentation of subduction zones and estimate the maximum possible size of earthquakes.

## Methods

**Seismic data acquisition and processing.** There are three problems that hinder the deep seismic imaging of structures below 10–15 km in subduction zone environments: (1) poor penetration of seismic energy through thick, highly attenuating sediments, (2) scattering of seismic energy from rough seafloor surfaces, where the water depth varies from 6 km to 50 m, and (3) reverberation of acoustic energy (water bottom multiples) in the water column. As high-frequency energy attenuates much faster than low-frequency energy, a low-frequency energy source is required for deep penetration. To remove multiples, long-offset data

are required<sup>21</sup>. The seafloor scattering is also less pronounced at long offsets. Most of the seismic experiments in the Sumatra region have used 2.4–3 km long streamers (ref. 18).

To overcome the above problems, CCGVeritas mobilized one of its largest seismic vessels, the Geowave Champion, towing a 15 km-long streamer that was five times larger than other surveys in the region. An array of 48 airguns with a total volume of 9,600 cubic inches was towed at 15 m water depth, providing the very large low-frequency energy source required to image deep targets. To enhance low frequencies further, the streamer was towed 22.5 m below the sea surface<sup>21</sup>, providing energy between 5 and 25 Hz. In conventional surveys, the streamer and airguns are generally deployed at 7–10 m water depths, providing energy between 10 and 70 Hz. We used a solid streamer instead of a fluid-filled streamer, leading to a further decrease in frequency down to 2 Hz. The receiver group interval was 12.5 m and the shot interval was 50 m, providing a fold of 300 (60 for 3 km long streamer), enhancing the signal-to-noise ratio significantly (which is essential for deep crustal imaging). The record length was 20 s, which corresponds to a depth of 55–60 km. The vessel speed was 4–4.5 knots. The survey was carried out in May 2009.

The data was processed using conventional processing techniques to enhance the low-frequency energy for deep imaging<sup>21</sup>. As the seafloor swell noise has frequencies up to 4 Hz, a special filter was designed to remove the swell noise while preserving the seismic signal down to 2 Hz. A combination of Radon multiple removal and surface-related multiple removal techniques was deployed. The velocity was determined using a combination of the constant velocity analysis technique and prestack time migration velocity analyses. The data was then migrated using a Kirchhoff time migration technique. An automatic gain control was applied and the results are shown in Figs 2 and 3.

**Earthquake relocation.** We used the method of Joint Hypocentre Determination (JHD; ref. 29), and P-wave arrival times reported by the International Seismological Centre (ISC) to relocate all seismicity between 1 January 1964 and 31 January 2008 in the area relative to the 12 September 2007,  $M_w$  8.4 earthquake. The ISC reports 4,865 earthquakes in the region 7.5–0.5° S, 97.5–103.5° E during this period, 337 of which have source mechanisms published by the Global CMT project. We successfully relocated 2,583 earthquakes. The proportion of earthquakes successfully relocated increases with time, reflecting improvements in instrumentation. We define earthquakes that we are able to relocate with the semi-major axis of their 90% error ellipse <30 km as being ‘reliably relocated’. A total of 917 earthquakes are thus reliably relocated, and plotted in Fig. 1 and Supplementary Fig. S4. All earthquakes with CMT solutions are reliably relocated, reflecting the superior quality data owing to their greater size. It is interesting that the ‘hole’ in the seismicity seen here is also visible at greater depths.

## References

- Cloos, M. Thrust type subduction zone earthquakes and seamount asperities: A physical model for earthquake rupture. *Geology* **20**, 601–604 (1992).
- Scholz, C. H. & Small, C. The effect of seamount subduction on seismic coupling. *Geology* **25**, 487–490 (1997).
- Kodaira, S., Takahashi, N., Nakanishi, A., Miura, S. & Kaneda, Y. Subducted seamount imaged in the rupture zone of the 1946 Nankaido earthquake. *Science* **289**, 104–106 (2000).
- Bilek, S. L., Schwartz, S. Y. & DeShon, H. R. Control of seafloor roughness on earthquake rupture behaviour. *Geology* **31**, 455–458 (2003).
- Robinson, D. P., Das, S. & Watts, A. B. Earthquake rupture stalled by subducting fracture zone. *Science* **312**, 1203–1205 (2006).
- Cummins, P. R., Baba, T., Kodaira, S. & Kaneda, Y. The 1946 Nankai earthquake and segmentation of the Nankai Trough. *Phys. Earth Planet. Int.* **132**, 75–87 (2002).
- Mochizuki, K., Yamada, T., Shinohara, M., Yamanaka, Y. & Kanazawa, T. Weak interplate coupling by seamounts and repeating  $M \sim 7$  earthquakes. *Science* **321**, 1194–1197 (2008).
- Abercrombie, R. E., Antolik, M. & Ekström, G. The June 2000  $M_w$  7.9 earthquake south of Sumatra: Deformation in the India–Australia Plate. *J. Geophys. Res.* **108**, 2018 (2003).
- Ranero, C.R. & van Huene, R. Subduction erosion along the Middle America convergent margin. *Nature* **404**, 748–752 (2000).
- Bangs, N. L. B., Gulick, S. P. S. & Shipley, T. H. Seamount subduction erosion in the Nankai Trough and its potential impact on the seismogenic zone. *Geology* **34**, 701–704 (2006).
- von Huene, R., Ranero, C. R. & Vannucchi, P. Generic model of subduction erosion. *Geology* **32**, 913–916 (2004).
- von Huene, R. When seamounts subduct. *Science* **321**, 1165–1166 (2008).
- Das, S. & Scholz, C. H. Why large earthquakes do not nucleate at shallow depth. *Nature* **305**, 621–623 (1983).
- Chlieh, M., Avouac, J.-P., Sieh, K., Natawidjaja, D. H. & Galetzka, J. Investigation of interseismic strain accumulation along the Sunda megathrust, offshore Sumatra. *J. Geophys. Res.* **113**, B05305 (2008).
- Konca, A. O. *et al.* Partial rupture of a locked patch of the Sumatra megathrust during the 2007 earthquake sequence. *Nature* **456**, 631–635 (2008).
- Fitch, T. J. Plate convergence, transcurrent faults, and internal deformation adjacent to Southeast Asia and the western Pacific. *J. Geophys. Res.* **77**, 4432–4462 (1972).
- Prawirodirdjo, L., McCaffrey, R., Chadwell, C. D., Bock, Y. & Subarya, C. Geodetic observation of an earthquake cycle at the Sumatra subduction zone: Role of interseismic strain segmentation. *J. Geophys. Res.* **115**, B03414 (2010).
- Kopp, H., Flueh, E., Klaeschen, D., Bialas, J. & Reichert, C. Crustal structure of the central Sunda margin at the onset of oblique subduction. *Geophys. J. Int.* **147**, 449–474 (2001).
- Singh, S. C. *et al.* Evidence of active backthrusting at the NE Margin of Mentawai Islands, SW Sumatra. *Geophys. J. Int.* **180**, 703–714 (2010).
- Chauhan, A. *et al.* Seismic imaging of forearc backthrusts at northern Sumatra subduction zone. *Geophys. J. Int.* **179**, 1772–1780 (2009).
- Singh, S. C. *et al.* Seismic evidence for broken oceanic crust in the 2004 Sumatra earthquake epicentral region. *Nature Geosci.* **1**, 777–781 (2008).
- Dessa, J.-X. *et al.* Megathrust earthquakes can nucleate in the forearc mantle: Evidence from the 2004 Sumatra event. *Geology* **37**, 659–662 (2009).
- Simoes, M., Avouac, J. P., Cattin, R. & Henry, P. Sumatra subduction zone: A case for a locked fault zone extending into the mantle. *J. Geophys. Res.* **109**, B10402 (2004).
- Schöffel, H.-J. & Das, S. Fine details of the Wadati–Benioff zone under Indonesia and its geodynamic implications. *J. Geophys. Res.* **104**, 13101–13114 (1999).
- Dominguez, S., Malavieille, J. & Lallemand, S. E. Deformation of accretionary wedges in response to seamount subduction: Insights from sandbox experiments. *Tectonics* **19**, 182–196 (2000).
- Slater, J. G. & Christie, P. A. F. Continental stretching: An explanation of the post–mid-Cretaceous subsidence of the Central North Sea basin. *J. Geophys. Res.* **85**, 3711–3739 (1980).
- Diament, M. *et al.* Mentawai fault zone off Sumatra—a new key to the geodynamics of western Indonesia. *Geology* **20**, 259–262 (1992).
- Cande, S. C. & Kent, D. V. Revised calibration of the geomagnetic polarity time scale for the late Cretaceous and Cenozoic. *J. Geophys. Res.* **100**, 6093–6095 (1995).
- Dewey, J. W. *Seismic Studies with the Method of Joint Hypocenter Determination*, PhD Thesis, Univ. of California, Berkeley (1971).

## Acknowledgements

We would like to thank the Chairman and CEO of CCGVeritas for supporting and funding the project. The Oxford group was partially supported by the UK Natural Environment Research Council grant NE/D004381/1. Institut de Physique du Globe contribution number 3131.

## Author contributions

S.C.S. led the project and wrote the paper. N.H. participated in the experiment and in writing the paper. M.M. and S.D. participated in writing the paper. D.P.R. relocated the earthquakes and participated in writing the paper. A.C., H.C., B.G. and Y.D. participated in the experiment. S.M. helped in designing the experiment. H.H. was instrumental in obtaining permits to acquire the data.

# SUPPLEMENTARY INFORMATION

## Aseismic zone and earthquake segmentation associated with a deep subducted seamount in Sumatra

### Supplementary Figure Legends

Figure 1S: **Bathymetry of the study area:** Dashed red line: Seismic profile CGGV040. Black dots mark the end positions of the imaged seamount (shown in Figure 2) along the seismic profile. The low bathymetry anomaly in the wake of the seamount is marked by thick white dashed line. Blue star: 2007 earthquake epicentre. GSF: Great Sumatra Fault. Black dashed lines (marked by A and B) indicate the location of bathymetric profiles shown in Figure 3. Yellow line: 1833 earthquake rupture zone. Pink line: Weakly coupled zone.

Figure S2: **Seismic Profile CGGV040:** Non-interpreted seismic image along profile CGGV040. The vertical to horizontal scale is 1:8 for a water velocity of 1.5 km/s.

Figure S3: **Blow-up of the seismic image of the seamounts:** Non-interpreted detailed profiles over seamounts along profile CGGV040 (a) and CGGV020 (b). The vertical to horizontal scale is 1:8 for a water velocity of 1.5 km/s. The location of the profile is shown in Figures 1 and 2.

Figure S4: **Relocated Epicentres:** Left Panels: 1 January 1964 until the 4 June 2000 earthquake (red star); Right panels: 4 June 2000 until 31 January 2008. Earthquakes with a Global Centroid Moment Tensor (GCMT) solution are shown in the lower panels as circles, and those without a GCMT as squares. The GCMT's shown in the upper panels are plotted at their relocated positions. The sizes of the circles and moment tensors scale with their reported  $M_w$ . Orange line: seismic profile CGGV040, black circles: edges of the seamount along the profile. Green dashed circle: zone without earthquakes > magnitude 5.

Figure S5: **Depth image along profile CGGV040:** The depth-converted image using a combination of velocity obtained from seismic reflection and that from (1). The hypocenters of the earthquakes<sup>1</sup> were projected along the profile within 20 km of the profile (black beach balls) and 60 km of the profile (red beach balls). This image was used to plot schematic diagram shown in Figure 4. The dashed black line shown in Figure 4 was obtained by connecting the hypocenters.

Figure S6: **Interpreted Depth image along profile CGGV040:** The depth-converted image using a combination of velocity obtained from seismic reflection and that from (1). The hypocenters of the earthquakes<sup>1</sup> were projected along the profile within 20 km of the profile (black beach balls) and 60 km of the profile (red beach balls). This image was used to plot schematic diagram shown in Figure 4. The main crustal-scale boundaries used in Figure 4 are in black, sediments in green and faults in red.

### Supplementary References

1. Engdahl, E.R., Villasenor, A., DeShon, H.R., and Thurber, C. H. Teleseismic relocation and assessment of seismicity (1918-2005) in the region of the 2004  $M_w$  9.0 Sumatra-Andaman and the 2005  $M_w$  8.6 Nias Island Great earthquakes. *Bull. Seism. Soc. Am.* **97**, S1-S19 (2007).

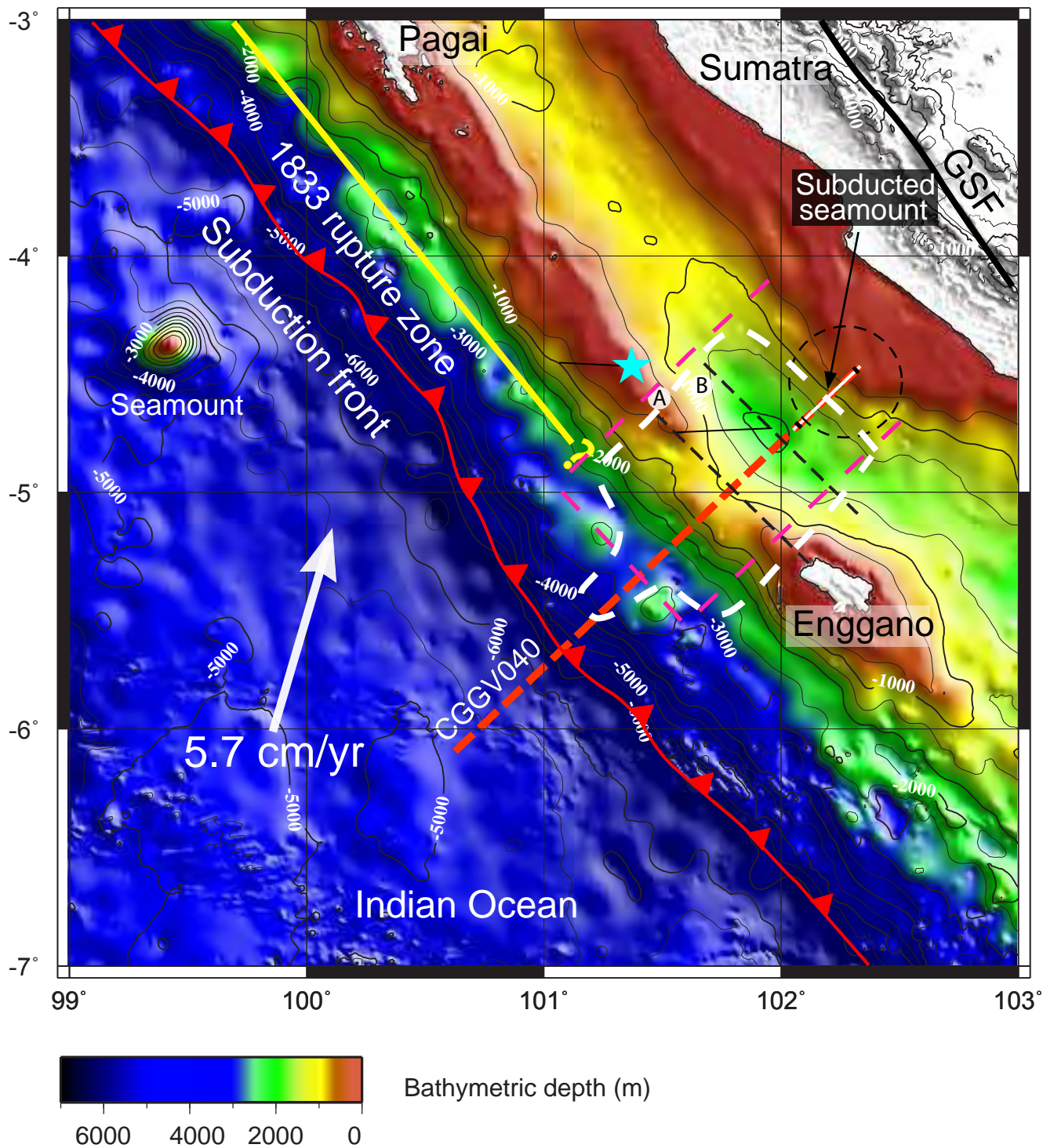


Figure S1 : **Bathymetry of the study area:** Dashed red line: Seismic profile CGGV040. Black dots mark the end positions of the imaged seamount (shown in Figure 2) along the seismic profile. The low bathymetry anomaly in the wake of the seamount is marked by thick white dashed line. Blue star: 2007 earthquake epicentre. GSF: Great Sumatra Fault. Black dashed lines (marked by A and B) indicate the location of bathymetric profiles shown in Figure 3. Yellow line: 1833 earthquake rupture zone. Pink line: Weakly coupled zone.

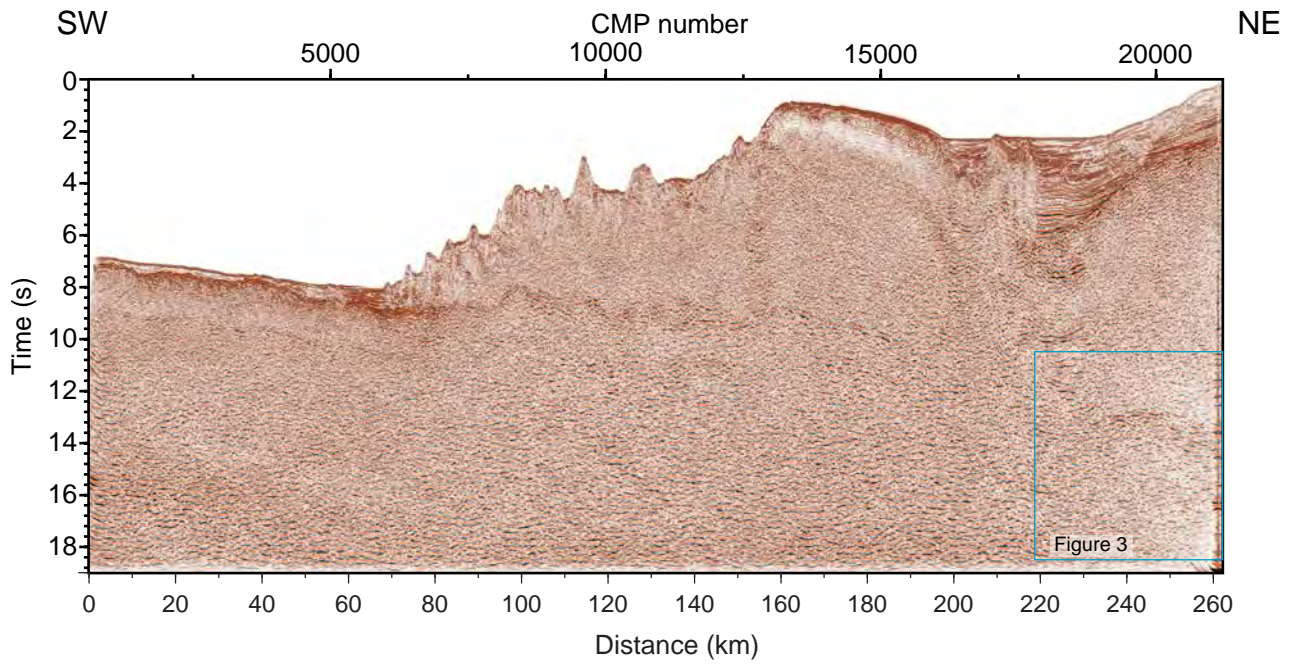


Figure S2: **Seismic Profile CGGV040**: Non-interpreted seismic image along profile CGGV040. The vertical to horizontal scale is 1:8 for a water velocity of 1.5 km/s.

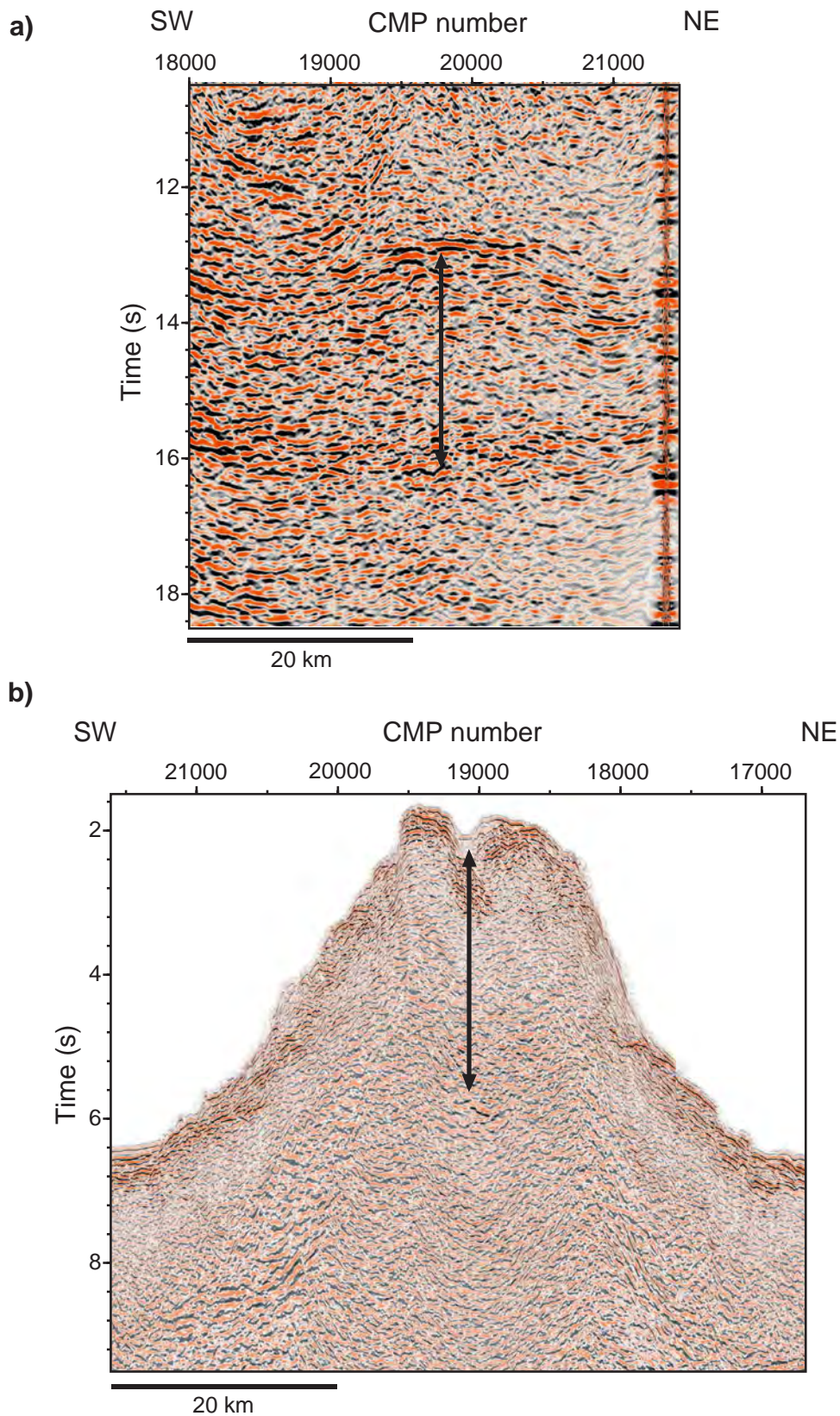


Figure S3: **Blow-up of the seismic image of the seamounts:** Non-interpreted detailed profiles over seamounts along profile CGGV040 (a) and CGGV020 (b). The vertical to horizontal scale is 1:8 for a water velocity of 1.5 km/s. The location of the profile is shown in Figures 1 and 2.



- 01/Jan/1964-04/Jun/2000
- 04/Jun/2000-26/Dec/2004
- 26/Dec/2004-28/Mar/2005
- 28/Mar/2005-12/Sep/2007
- 12/Sep/2007-12/Sep/2007
- 12/Sep/2007-31/Jan/2008

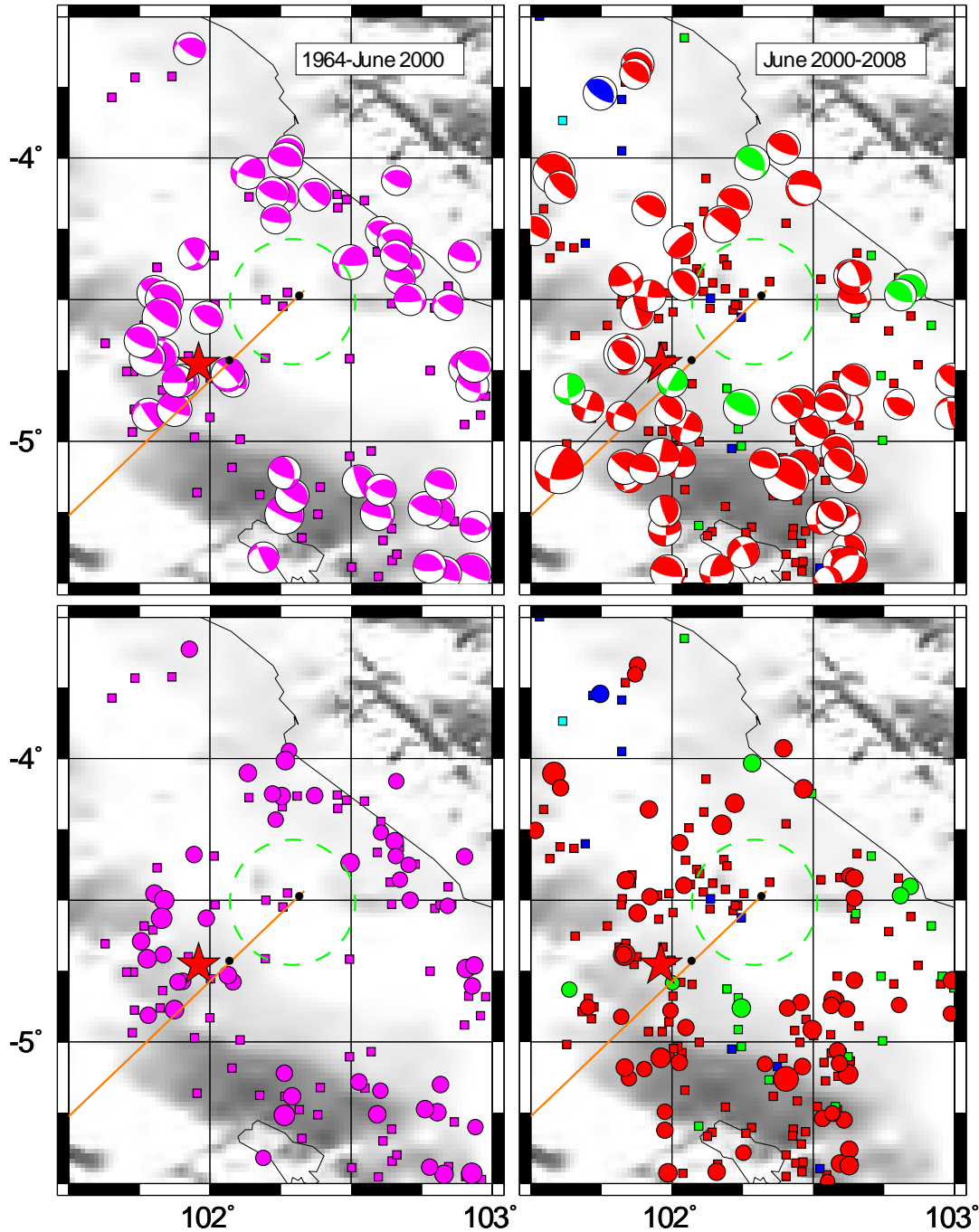


Figure S4: **Relocated Epicentres**: Left Panels: 1 January 1964 until the 4 June 2000 earthquake (red star); Right panels: 4 June 2000 until 31 January 2008. Earthquakes with a Global Centroid Moment Tensor (GCMT) solution are shown in the lower panels as circles, and those without a GCMT as squares. The GCMT's shown in the upper panels are plotted at their relocated positions. The sizes of the circles and moment tensors scale with their reported  $M_w$ . Orange line: seismic profile CGGV040, black circles: edges of the seamount along the profile. Green dashed circle: zone without earthquakes > magnitude 5.

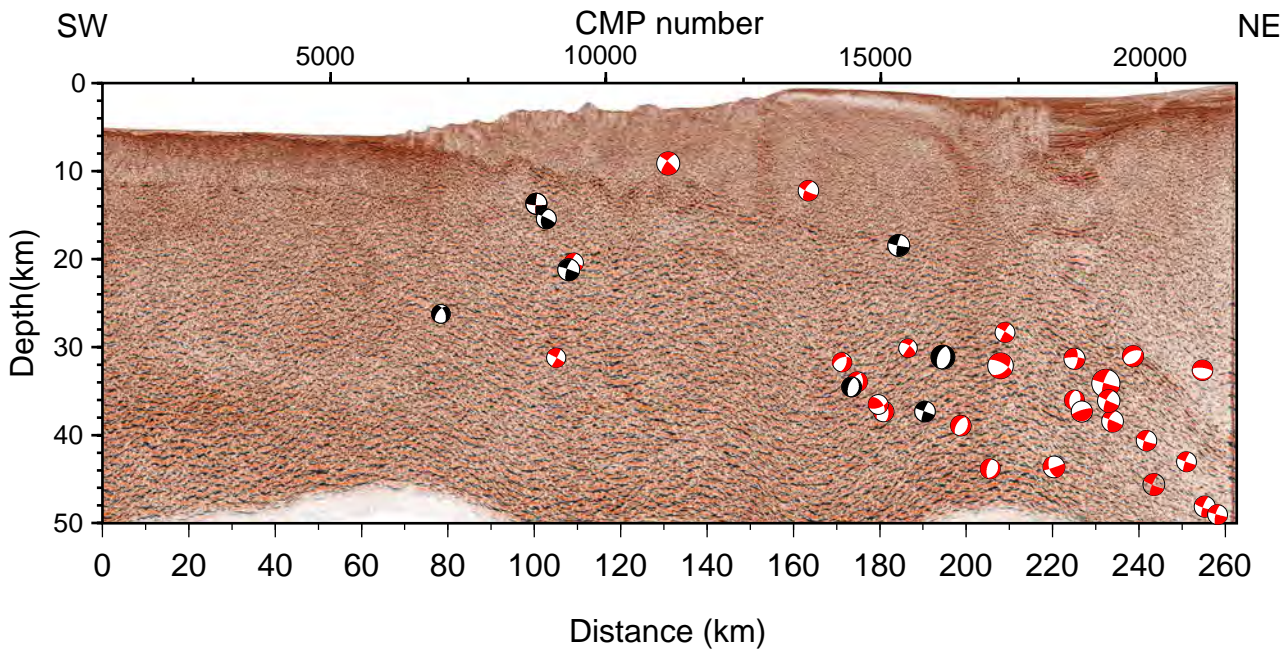


Figure S5: **Depth image along profile CGGV040:** The depth-converted image using a combination of velocity obtained from seismic reflection and that from (1). The hypocenters of the earthquakes<sup>1</sup> were projected along the profile within 20 km of the profile (black beach balls) and 60 km of the profile (red beach balls). This image was used to plot schematic diagram shown in Figure 4. The dashed black line shown in Figure 4 was obtained by connecting the hypocenters.

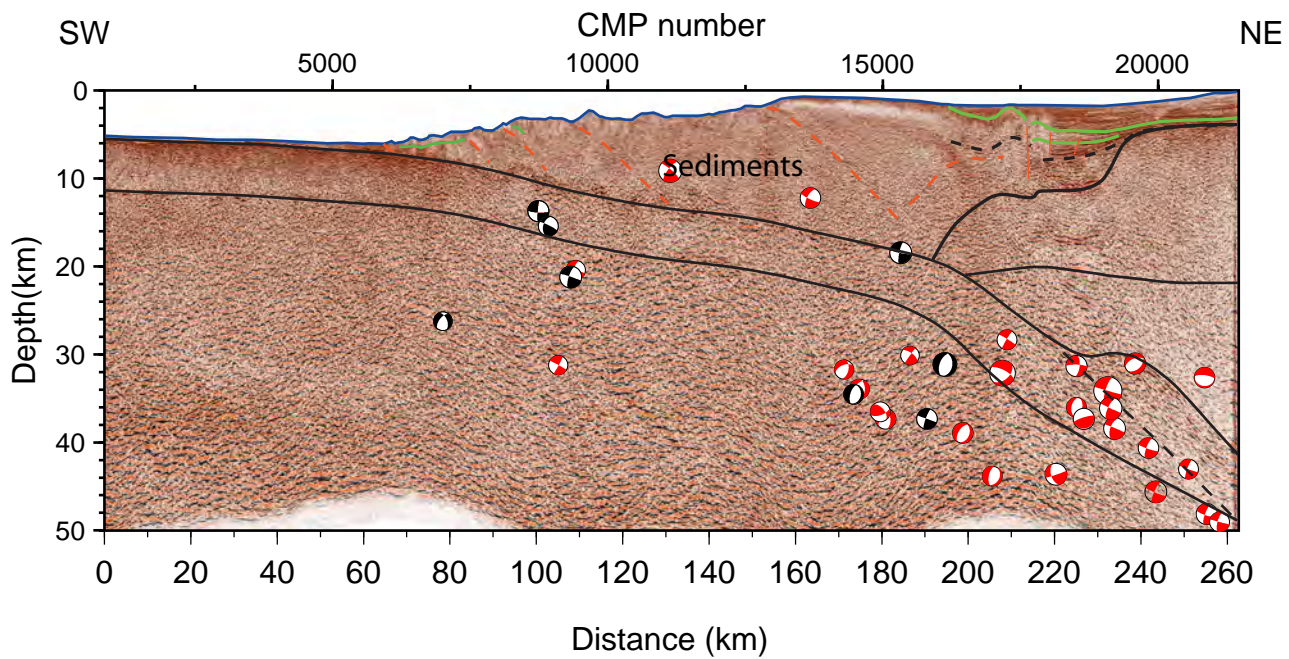


Figure S6: **Interpreted Depth image along profile CGGV040:** The depth-converted image using a combination of velocity obtained from seismic reflection and that from (1). The hypocenters of the earthquakes<sup>1</sup> were projected along the profile within 20 km of the profile (black beach balls) and 60 km of the profile (red beach balls). This image was used to plot schematic diagram shown in Figure 4. The main crustal-scale boundaries used in Figure 4 are in black, sediments in green and faults in red.